



INSTITUT DE FRANCE
Académie des sciences

Comptes Rendus

Géoscience

Sciences de la Planète

Thibault Mathevet, Nicolas Le Moine, Vazken Andréassian, Hoshin Gupta
and Ludovic Oudin

**Multi-objective assessment of hydrological model performances using
Nash–Sutcliffe and Kling–Gupta efficiencies on a worldwide large sample of
watersheds**

Volume 355, Special Issue S1 (2023), p. 117-141


Online since: 24 January 2023

Issue date: 23 February 2024

Part of Special Issue: Geo-hydrological Data & Models

Guest editors: Vazken Andréassian (INRAE, France),
Valérie Plagnes (Sorbonne Université, France), Craig Simmons (Flinders University,
Australia) and Pierre Ribstein (Sorbonne Université, France)

<https://doi.org/10.5802/crgeos.189>

 This article is licensed under the
CREATIVE COMMONS ATTRIBUTION 4.0 INTERNATIONAL LICENSE.
<http://creativecommons.org/licenses/by/4.0/>



*The Comptes Rendus. Géoscience — Sciences de la Planète are a member of the
Mersenne Center for open scientific publishing*

www.centre-mersenne.org — e-ISSN : 1778-7025



Research article

Geo-hydrological Data & Models

Multi-objective assessment of hydrological model performances using Nash–Sutcliffe and Kling–Gupta efficiencies on a worldwide large sample of watersheds

Thibault Mathevet^{Ⓜ,*,a,b}, Nicolas Le Moine^{Ⓜ,c}, Vazken Andréassian^{Ⓜ,d}, Hoshin Gupta^{Ⓜ,e}
and Ludovic Oudin^{Ⓜ,c}

^a EDF, 4 allée du Lac de Tignes, 73290 La Motte Servolex, France

^b Visiting research scholar at Hydrology and Atmospheric Sciences, University of Arizona, in 2014

^c Sorbonne Université, CNRS, EPHE, UMR 7619 METIS, Case 105, 4 place Jussieu, 75005 Paris, France

^d Université Paris-Saclay, INRAE, UR HYCAR, 1 Rue Pierre-Gilles de Gennes, 92160 Antony, France

^e Department of Hydrology and Atmospheric Sciences, University of Arizona, Tucson, AZ, USA

E-mails: thibault.mathevet@edf.fr (T. Mathevet),
nicolas.le_moine@sorbonne-universite.fr (N. Le Moine), vazken.andreassian@inrae.fr
(V. Andréassian), hoshin@arizona.edu (H. Gupta),
ludovic.oudin@sorbonne-universite.fr (L. Oudin)

Abstract. We introduce a new diagnosis tool that is well suited to analyzing simulation results over large samples of watersheds. It consists of a modification of the classical Taylor diagram to simultaneously visualize several error components (based on bias, standard deviation or squared errors) that are commonly used in efficiency criteria (such as the Nash–Sutcliffe efficiency (NSE) or the Kling–Gupta efficiency (KGE)) to evaluate hydrological model performance. We propose a methodological framework that explicitly links the graphical and numerical evaluation approaches, and show how they can be usefully combined to visually interpret numerical experiments conducted on large datasets. The approach is illustrated using results obtained by testing two rainfall-runoff models on a sample of 2050 watersheds from 8 countries and calibrated with two alternative objective functions (NSE and KGE). The assessment tool clearly highlights well-documented problems related to the use of the NSE for the calibration of rainfall-runoff models, which arise due to interactions between the ratio of simulated to observed standard deviations and the correlation coefficient. We also illustrate the negative impacts of classical mathematical transformations (square root) applied to streamflow when employing NSE and KGE as metrics for model calibration.

* Corresponding author.

Keywords. Hydrological modeling, Large-sample hydrology, Taylor diagram, Diagnostics, Kling–Gupta efficiency, Nash–Sutcliffe efficiency.

Manuscript received 7 April 2022, revised 30 August 2022 and 27 October 2022, accepted 24 November 2022.

1. Introduction

Hydrological models are widely used for research, engineering and water resources management. Whatever the context, modelers often share common interests in quantifying the efficiency, the robustness and the realism of models structures, improving the generality and transposability of model structures across space and time scales, and designing methods to extract information from hydrological time series for model parameter identification.

A wide panel of methodologies and numerical techniques currently exist to meet these objectives. But advanced model validation remains a key issue for model users, who apply models to make decisions. The balance between the predictive power and the physical realism of models is still a matter of debate in validation approaches (see for example the debate between Konikow and Bredehoeft [1992] and de Marsily [1994], as summarized by Andréassian [2023], this issue). In the context of growing data availability [Addor *et al.*, 2020], the efficiency and generality of models can be better assessed by using large watershed samples [Gupta *et al.*, 2014], typically consisting of several hundreds to a few thousands of watersheds [Newman *et al.*, 2015, McMillan *et al.*, 2016, Lane *et al.*, 2019, Mathevet *et al.*, 2020]. The use of large watershed samples has various benefits, among which are improved understanding based on rigorous and controlled numerical experiments allowing comparison and hypothesis testing, and improved robustness of generalization based on statistical analyses of model performance and reduced sensitivity to site-specific watershed properties.

Among the efficiency criteria commonly used to quantify the adequacy between simulations and observations, the Nash–Sutcliffe efficiency [Nash and Sutcliffe, 1970; NSE] and the Kling–Gupta efficiency [Gupta *et al.*, 2009; KGE] provide summary statistics that can be calculated on long periods or sub-periods [Mathevet *et al.*, 2020]. These metrics are often applied to model simulations considering as target variables: (i) streamflow (Q), (ii) various non-linear transformations of streamflow [square root, inverse, logarithmic or Box–Cox transformations; see Santos

et al., 2018] and (iii) some hydrological signatures (hydrological regime, flood distribution, drought distribution, etc.). Some major drawbacks of the NSE have long been demonstrated: the use of a poor benchmark model to assess model performances [Schaeffli and Gupta, 2007], an unbounded formulation inappropriate for statistical analyses [Mathevet *et al.*, 2006] or an unpredictable trade-off between mean bias, variability bias and correlation while calibration [Gupta *et al.*, 2009]. The KGE has been proposed to overcome some of these problems, providing a more balanced compromise between expected properties of model simulations (bias on mean flow, bias on flow variability and correlation between simulation and observation).

When working with large watershed samples, it becomes necessary to summarize the sets of efficiency criteria values to enable effective comparison of performance obtained with different model structures, time periods or calibration options, etc. Distributions, boxplots and scatterplots are often used to visually compare numerical experiments. However, while such analyses are statistically relevant, they can drastically reduce the information content of a numerical experiment, particularly when some criteria are partially correlated. Alternatively, one may consider the Taylor diagram [Taylor, 2001], which is commonly used to simultaneously visualize several error components of a model simulation, and which has been used in climate and hydrological modeling studies. Taylor diagram is usually used in its classical formulation to compare few models or few data sets on a case study, considering correlation, standard deviation and root mean square error (RMSE) [Yaseen *et al.*, 2018, Maroufpoor *et al.*, 2020].

The objective of this paper is to propose a modification of Taylor diagram to simultaneously represent components of the KGE, i.e. mean bias, variability bias and correlation. We illustrate the application of this graphical tool using results of a numerical experiment based on the methodology proposed by Mathevet *et al.* [2020] and demonstrate its usefulness to answer the following research questions:

- What are the main performances of models calibrated using NSE or KGE as objective

function (in terms of mean bias, standard deviation bias and correlation and dependency structure between these criteria)?

- Do the performances vary with model structure or watershed location?
- What are the impacts of non-linear transformations of streamflow, classically used when calibrating rainfall-runoff models?

Section 2 presents the theoretical background of Taylor diagram and its modification, Section 3 presents an overview of the experimental design, and Section 4 details the general results of the study. Section 5 presents a discussion of the results and our conclusions are given in Section 6.

2. Theoretical background

2.1. Classical Taylor diagram

This section reviews the basics underlying the construction of a Taylor diagram. Table 1 lists the symbols used throughout this paper.

A Taylor diagram [Taylor, 2001] is intended to simultaneously display several metrics on a graph, describing the discrepancies between a test field or series (e.g., the simulation) and a reference one (e.g., the observation). These metrics consist of the (sample) Pearson correlation coefficient R , the standard deviation of the simulation $\hat{\sigma}$ (resp. the ratio of simulated to observed standard deviation $\hat{\sigma}/\sigma_0$), and E' the root mean squared error on centered patterns (CRMSE). The CRMSE differs from E , the classical RMSE, in the removal of the bias component, according to the relation:

$$E^2 = \frac{1}{n} \sum_{i=1}^n [\hat{f}_i - f_i]^2 \quad (1)$$

$$E^2 = \frac{1}{n} \sum_{i=1}^n [(\hat{f}_i - \hat{\mu}) - (f_i - \mu_0) + (\hat{\mu} - \mu_0)]^2 \quad (2)$$

$$E^2 = \frac{1}{n} \sum_{i=1}^n [(\hat{f}_i - \hat{\mu}) - (f_i - \mu_0)]^2 + \frac{2}{n} (\hat{\mu} - \mu_0) \times \left[\sum_{i=1}^n (\hat{f}_i - \hat{\mu}) - \sum_{i=1}^n (f_i - \mu_0) \right] + (\hat{\mu} - \mu_0)^2 \quad (3)$$

with

$$E'^2 = \frac{1}{n} \sum_{i=1}^n [(\hat{f}_i - \hat{\mu}) - (f_i - \mu_0)]^2. \quad (4)$$

By definition of the sample mean, the terms $\sum_{i=1}^n (\hat{f}_i - \hat{\mu})$ and $\sum_{i=1}^n (f_i - \mu_0)$ sum up to zero, so that Equation (3) can be simplified to:

$$E^2 = E'^2 + (\hat{\mu} - \mu_0)^2 = E'^2 + \beta^2. \quad (5)$$

By further developing E'^2 we get:

$$E'^2 = \frac{1}{n} \sum_{i=1}^n (\hat{f}_i - \hat{\mu})^2 + \frac{1}{n} \sum_{i=1}^n (f_i - \mu_0)^2 - 2 * \frac{1}{n} \sum_{i=1}^n (\hat{f}_i - \hat{\mu})(f_i - \mu_0) \quad (6)$$

$$E'^2 = \hat{\sigma}^2 + \sigma_0^2 - 2 * \hat{\sigma} \sigma_0 R \quad (7)$$

or its normalized version:

$$\left(\frac{E'}{\sigma_0} \right)^2 = \left(\frac{\hat{\sigma}}{\sigma_0} \right)^2 + 1 - 2 * \frac{\hat{\sigma}}{\sigma_0} R. \quad (8)$$

If we define a polar plane such that a given simulation is represented by the point P : ($\rho = \hat{\sigma}$; $\theta = \arccos R$), then according to the law of cosines, the third metric E' is given by the distance between P and the reference point P_0 : ($\rho = \sigma_0$; $\theta = 0$) located on the cartesian x -axis. The same plot can be drawn using normalized values, the simulation and reference points being respectively defined by P' : ($\rho = \hat{\sigma}/\sigma_0$; $\theta = \arccos(R)$) and P_0 : ($\rho = 1$; $\theta = 0$).

2.2. Adapting Taylor diagram to represent bias, NSE, total RMSE, or any monotonic function of sum of squared errors (SSE)

One limitation of the previous diagram is that it does not allow for visualizing the absolute bias along with the CRMSE, and not the bias component $\beta = \mu_0 - \hat{\mu}$ (resp. $\beta_n = (\mu_0 - \hat{\mu})/\sigma_0$). Though it is rarely used in the literature, Taylor proposed a method to display bias on the same frame. It consists of attaching a segment to the point, which length is equal to $|\beta|$ (resp. $|\beta_n|$ in the normalized version), as shown in Figure 1.

If the segment is oriented perpendicular to the direction (P_0P), then the squared hypotenuse $P_0P'^2$ of the right triangle created in this way satisfies the condition:

$$P_0P'^2 = P_0P^2 + PP'^2 \quad (9)$$

$$P_0P'^2 = E'^2 + \beta^2 \quad (10)$$

$$P_0P'^2 = E^2. \quad (11)$$

If we chose to normalize errors with the standard deviation σ_0 of the observed streamflow series, the squared hypotenuse $P_0P'^2$ now quantifies the total

Table 1. List of symbols used

Symbol	Meaning	Mathematical definition
μ_0	Mean of observed streamflow	
$\hat{\mu}$	Mean of simulated streamflow	
σ_0	Standard deviation of observed streamflow	
$\hat{\sigma}$	Standard deviation of simulated streamflow	
β	Absolute mean bias	$\beta = \mu_0 - \hat{\mu}$
β_n	Normalized mean bias	$\beta_n = \frac{\mu_0 - \hat{\mu}}{\sigma_0}$
β_r	Relative mean bias	$\beta_r = \frac{\hat{\mu}}{\mu_0}$
α	Relative variability bias	$\alpha = \frac{\hat{\sigma}}{\sigma_0}$
E	Root mean square error (RMSE)	
E'	RMSE on centered patterns (CRMSE)	$E'^2 = E^2 - \beta^2$
ρ	Radius (distance to origin) in the polar plane	
θ	Azimuth (counter-clockwise from x -axis)	
R	Pearson correlation coefficient	
f_i	Observations of a given variable (streamflow in our case)	
\hat{f}_i	Estimations of a given variable	

normalized squared error and Equations (10) and (11) become respectively Equations (12) and (13):

$$P_0 P'^2 = \left(\frac{E'}{\sigma_0}\right)^2 + \beta_n^2 \quad (12)$$

$$P_0 P'^2 = \left(\frac{E}{\sigma_0}\right)^2 \quad (13)$$

which means that with P' we now have a reading of both bias ($|\beta|$, leg PP' of the right triangle) and total RMSE (E , hypotenuse P_0P'). Since the segment representing bias only has to be at a right angle with the segment reaching the reference, then we can for example choose a clockwise rotation for negative bias (i.e., an arrow pointing towards $-P'$, the origin of the polar plane) and counterclockwise for positive bias (i.e., an arrow pointing towards P' , the outer boundary).

Recognizing that NSE, MSE, RMSE are all monotonic functions of the total sum of squared errors, it is then easy to modify the diagram in order to display curves that are, for example, contour lines of NSE efficiency or its bounded version [Mathevet *et al.*, 2006] rather than contour lines of (C)RMSE. In this section, we show that any monotonic function of SSE

can be drawn on the normalized version of the Taylor diagram. This provides an interesting outlook of a hydrological simulation through the visualization of five assessment criteria for all the watersheds: correlation R , ratio of simulated to observed standard deviation, normalized bias β_n , NSE on centered patterns (CNSE) and classical NSE.

2.3. Prone-like regions in the modified Taylor diagram depending on the objective function

We now wish to determine in which region of the Taylor diagram a simulation result should fall, when the hydrological model is calibrated with an ordinary-least-squares (OLS) criterion such as the Nash–Sutcliffe efficiency.

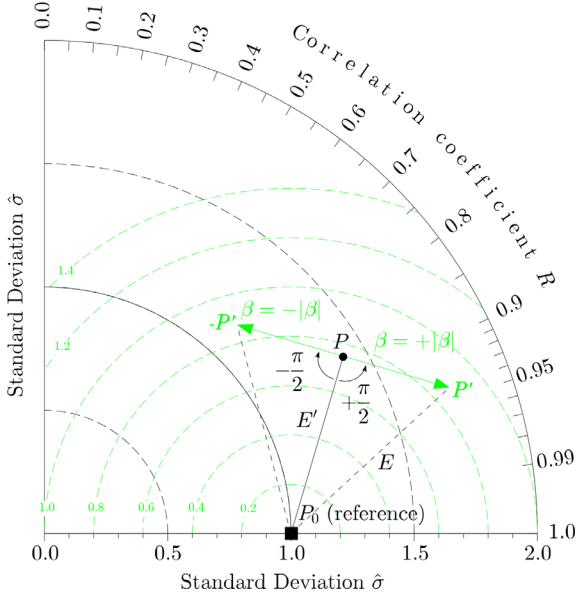


Figure 1. Convention for representing bias and total RMSE. Green circles centered on the reference are contours of CRMSE if used with the dot P , or RMSE if used with the end tip of the green arrow (P'). In this case where $\sigma_0 = 1$ for the sake of simplicity, estimated standard deviation is $\hat{\sigma} = 1.41$, correlation $R = 0.86$, CRMSE $E' = 0.75$, bias $\beta = \pm 0.45$ and RMSE $E = 0.87$.

For this, we use the decomposition of NSE proposed by Gupta *et al.* [2009], which reads:

$$\text{NSE} = 1 - \left(\frac{E}{\sigma_0}\right)^2 \quad (14)$$

$$\text{NSE} = 1 - \left(\frac{E'}{\sigma_0}\right)^2 + \beta_n^2 \quad (15)$$

$$\text{NSE} = 2\left(\frac{\hat{\sigma}}{\sigma_0}\right)R - \left(\frac{\hat{\sigma}}{\sigma_0}\right)^2 - \beta_n^2 \quad (16)$$

$$\text{NSE} = 2\alpha R - \alpha^2 - \beta_n^2. \quad (17)$$

Equations (14)–(17) show that OLS-like criteria tend to fit the first ($\beta = \beta_n = 0$ or in other words $E = E'$) and second ($\alpha = 1$) moments of the distribution of the observations in a rather straightforward way. Conversely, the role of the correlation term R that represents the ability of the model to reproduce timing and shape is mixed up with the value of α . This appears clearer when deriving Equation (15) with respect to α by considering R and β_n fixed, as shown by Gupta

et al. [2009]:

$$\frac{\partial \text{NSE}}{\partial \alpha} = 2(R - \alpha) = 0. \quad (18)$$

Hence, any OLS calibration will tend to equate α , the ratio of simulated to observed standard deviation, with the correlation coefficient R : these two metrics are entangled. This also poses a problem since R is necessarily lesser than unity, OLS calibration will lead to α less than unity, i.e. a systematic underestimation of the variance of streamflow. We will show how this dependency should translate in the Taylor diagram.

Let us consider the normalized version of the Taylor diagram, and let ε_{OLS} be the locus of the points satisfying the condition $\alpha = R$ i.e. $\theta = \arccos(R) = \arccos(\alpha)$. The cartesian coordinates of those points hence verify:

$$x = \alpha \cdot \cos(\theta) = \alpha \cdot \cos(\arccos(\alpha)) = \alpha^2 \quad (19)$$

$$y = \alpha \cdot \sin(\theta) = \alpha \cdot \sin(\arccos(\alpha)). \quad (20)$$

It is then easy to see that ε_{OLS} is the semi-circle centered at $(x = 1/2; y = 0)$, with radius $1/2$. Indeed, for any point in ε_{OLS} we have:

$$\left(x - \frac{1}{2}\right)^2 + y^2 = x^2 - x + \frac{1}{4} + y^2 \quad (21)$$

$$\left(x - \frac{1}{2}\right)^2 + y^2 = \alpha^4 - \alpha^2 + \frac{1}{4} + \alpha^2 \sin^2(\arccos(\alpha)) \quad (22)$$

$$\begin{aligned} \left(x - \frac{1}{2}\right)^2 + y^2 &= \alpha^2(\alpha^2 - 1) \\ &\quad + \frac{1}{4} + \alpha^2(1 - \cos^2(\arccos(\alpha))) = \frac{1}{4}. \end{aligned} \quad (23)$$

This result is illustrated in Figure 2. For every point of this circle (red dots), the radial through this point (red dashed line) is tangent to the NSE (or RMSE, or SSE, etc.) contour passing through this same point (green dash circle). We can call this curve the “*least-squares attractor in the absence of bias*” and in the following sections we will show that indeed models calibrated with a monotonic function of the sum of squared errors tend to align along this semi-circle in the polar plane. Since the red curve is systematically under the ideal fit of normalized standard deviation ($\alpha = (\hat{\sigma}/\sigma_0) = 1$), this illustrates the inherent problems of underestimation of the variance of OLS schemes. As a consequence of the normalization of the axes of standard deviation, the green dashed lines now represent isolines of NSE, instead of the isolines of RMSE in Figure 1. Figure 2 shows clearly the unfair trade-off occurring during an OLS

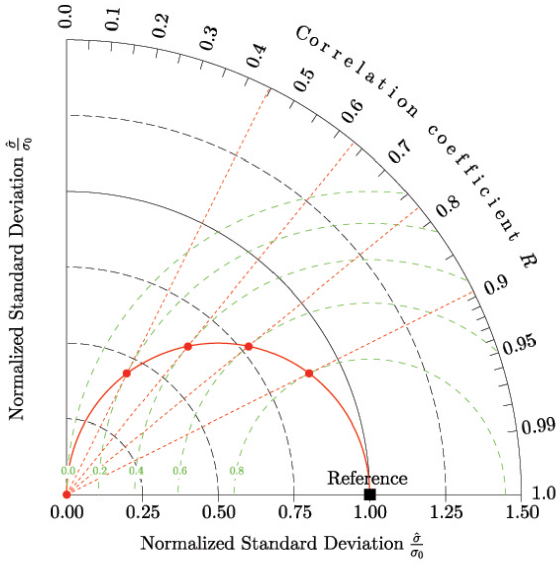


Figure 2. Construction of the locus of the points satisfying $\partial\text{NSE}/\partial\alpha = 0$ or, synonymously, $\alpha = R$ in red. The green circles are contours of NSE.

scheme between R and the ratio of standard deviation since the least-squares attractor tends to favor a higher correlation at the expense of a systematic underestimation of α . In its present form, note that the proposed modified Taylor diagram does not allow the representation of negative NSE. This was also a problem with the classical Taylor diagram that does not allow the representation of a negative correlation coefficient.

3. Experimental design

Here we use the same numerical experiment as in Mathevet *et al.* [2020], which is briefly summarized in this section.

3.1. Watershed sample

A large sample of 2050 watersheds spanning over eight countries is used in this paper. This sample is mainly (80%) represented by watersheds in France, USA and Australia. Other watersheds are situated in Italy, Laos, Sweden, Switzerland and UK. This sample covers a variety of climatological, physical and

hydrological characteristics (see Table 2). Time series consisted of mean daily rainfall, air temperature and streamflow. Climatic data are averages at the watershed scale, but the way these averages were computed is variable between the national sub-samples of watersheds. Potential evapotranspiration (PE) was computed using the temperature-based formula proposed by Oudin *et al.* [2005].

3.2. Hydrological models

Two conceptual rainfall-runoff models are used in this study: the GRX model [slightly modified from GR4J model, Le Moine, 2008 and Pushpalatha *et al.*, 2011] and the MRX model [modified from MOR-DOR model, Garçon, 1996 and Garavaglia *et al.*, 2017]. These two models have already been intensively tested, both for research and operational applications, in France and worldwide [Mathevet *et al.*, 2020]. A number of studies have shown that their structures can be efficient, with comparable performance in simulation, forecast and extrapolation modes. A snow accumulation and melt routine [from Garavaglia *et al.*, 2017] is also used in this study to represent snow processes of mountainous watersheds. Note that these two models differ in their level of complexity with 9 free parameters for GRX and 22 free parameters for MRX.

3.3. Calibration and evaluation metrics

Two classical metrics were used:

- Nash–Sutcliffe efficiency (Equation (14));
- Kling–Gupta efficiency (Equation (24));

$$\text{KGE} = 1 - \sqrt{(\beta_r - 1)^2 + (\alpha - 1)^2 + (R - 1)^2}, \quad (24)$$

where β_r and α assess the mean and variability bias of the long-term water balance, while R assesses the temporal dynamics of model simulations.

NSE and KGE metrics were used for model calibration. NSE, KGE, β_r , α and R were used for model evaluation. On a limited sub-sample of 635 watersheds (30% of the whole sample, to reduce computing time), a square root transformation of streamflow time-series was used to compute NSE and KGE metrics for model calibration.

Table 2. Distributions of characteristics of the 2050-watershed sample

Characteristics	Distribution percentiles				
	0.05	0.25	0.50	0.75	0.95
Watershed area (km ²)	31	102	255	734	2785
Mean annual total precipitation (P) (mm/yr)	626	800	950	1175	1627
Part of precipitation falling as snow (-)	0	0	0.03	0.09	0.29
Mean annual air temperature (°C)	4.9	9.2	10.5	12.1	16.2
Mean annual potential evapotranspiration (PE) (mm/yr)	471	633	686	773	998
Mean annual runoff (Q) (mm/yr)	53	207	344	541	1111
Aridity index (P/PE) (-)	0.80	1.12	1.35	1.74	2.82
Runoff coefficient (Q/P) (-)	0.08	0.24	0.36	0.48	0.79
Available time series length (yr)	11	18	33	36	55

3.4. Testing procedure

A classical split sample test (SST) procedure was implemented [Klemeš, 1986]. For each watershed, the available time period was divided into two independent sub-periods of equivalent length. After a one-year warm-up period to minimize state initialization errors, calibration was performed on each sub-period (first half, then second half), followed by evaluation on the other sub-period (second half, then first half). On the 2050 watershed sample, the mean temporal length of calibration and evaluation periods is 14 years. This testing procedure provided 4100 calibration and evaluation periods to assess model performance. Parameter optimization was conducted by use of a genetic algorithm [Mathevet, 2005].

4. Results

4.1. Mono-objective performance assessment using distribution or boxplot analyses

When using a large sample of watersheds, it is difficult to focus on local performance of a given model on a particular watershed, but much easier to draw general conclusions regarding comparative model performance under the hypotheses of the numeric experiments studied. Classically, samples of performance metrics are analyzed using empirical cumulative distributions (Figure 3) and distributions are summarized by boxplots (Figure 4).

Figure 3 shows the full distribution for the KGE(Q) performance metric only (for sake of brevity), while models are calibrated with NSE(Q) (Figure 3a) and KGE(Q) (Figure 3b). This figure shows that models have a similar distribution of KGE(Q) (particularly above median value) in calibration and evaluation, that models have a similar reduction of performance from calibration to evaluation and obviously that models calibrated with KGE(Q) have better performances than models calibrated with NSE(Q), while evaluated with KGE(Q).

Figure 4 shows the sample distributions of performance metrics (β_r , α , R , KGE and NSE) for the calibration and evaluation periods (i.e. 4100 values per period), for each of the two models calibrated either with NSE(Q) or KGE(Q) as objective function (a detailed analysis of this numerical experiment is presented in Mathevet et al. [2020]).

When using NSE(Q) as objective function, Figure 4a shows that models are not biased in terms of mean calibration. During evaluation, models could be biased in mean but they remain not biased on average (instead the spread of the distribution increases). In terms of variability bias, Figure 4a shows that models are biased on average (mean underestimation of variability by 10%) and that the spread of the variability bias distribution increases from calibration to evaluation [Gupta et al., 2009].

When using KGE(Q) as objective function, Figure 4b shows that models are not biased in terms of mean and variability during calibration. During evaluation, models could be biased in mean and variabil-

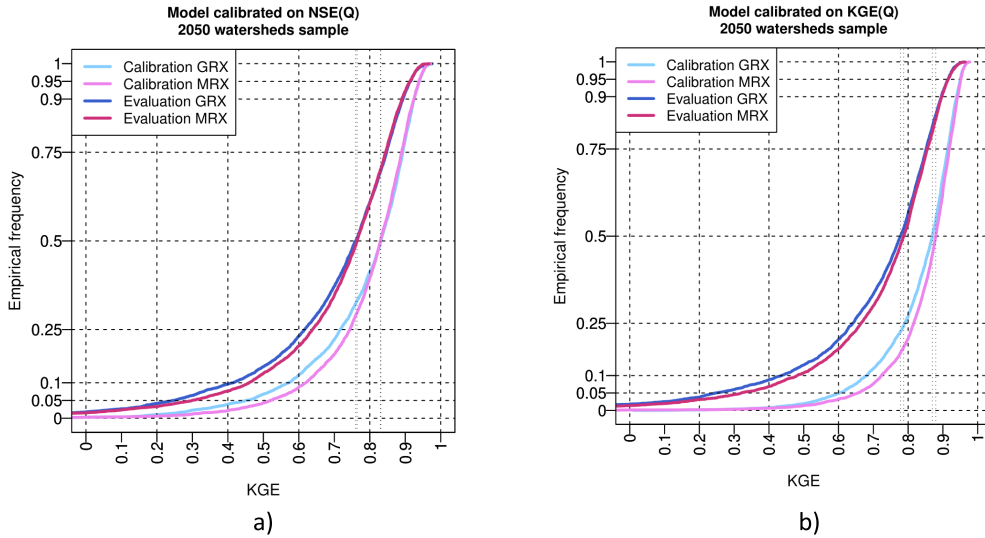


Figure 3. Comparison of GRX and MRX KGE performance in calibration and evaluation using (a) NSE(Q) or (b) KGE(Q) as objective function to optimize model parameters.

ity, but they remain not biased on average (the spread of the distribution increases).

Figure 4 also shows that both models have a median correlation around 0.9 and that distributions are pretty similar for the two models and from calibration to evaluation. This means that the watershed dynamics are rather equally well represented by both models, whatever the objective function used for optimization.

KGE(Q) and NSE(Q) distributions partially filter out some important features of individual mean and variability bias distributions and correlation distribution. While calibrated with KGE(Q), the KGE(Q) distribution is very similar to the correlation distribution since models are not biased in terms of mean and variability. From calibration to evaluation, both KGE(Q) and NSE(Q) distributions show a general decrease due to the average decline of performance concerning the representation of streamflow mean and variability.

4.2. Multi-objective performance assessment using Taylor diagram

In the following part of the paper, only GRX results will be presented, since the MRX results have similar patterns and lead to similar conclusions. MRX results are presented in Appendix A.

Distributions or boxplots are useful graphical tools for the statistical analysis of model performance for a given metric. However as stated earlier (Section 2), some performance metrics might be correlated while calibrated with a given objective function (NSE(Q) as an example, or any OLS criterion).

Figure 5a shows the GRX model results when calibrated with NSE(Q) as objective function. This figure confirms that the theoretical behavior described earlier by Gupta *et al.* [2009] actually occurs when calibrating the model with the NSE(Q) criterion. In the calibration phase, hydrological models manage to get a quite small mean bias, since red arrows are barely distinguished in the left-hand side diagram of Figure 5a, given that they are very short. Mean bias in calibration is becoming greater for watersheds where models obviously fail to correctly simulate streamflow. It is generally the case of very arid watersheds, where models are less robust, with lower correlation and higher standard deviation bias [Mathevet *et al.*, 2020]. RMSE and CRMSE being very close for most of the watersheds, the colored dots characterizing the centered patterns clearly align along the blue semi-circle in the (R, α) space, where the condition $\alpha = \hat{\sigma}/\sigma_0 = R$ is satisfied. Two-dimensional contour plots show that 90% of the population lies between $R \in [0.6, 0.98]$ and $\alpha \in [0.5, 1.02]$.

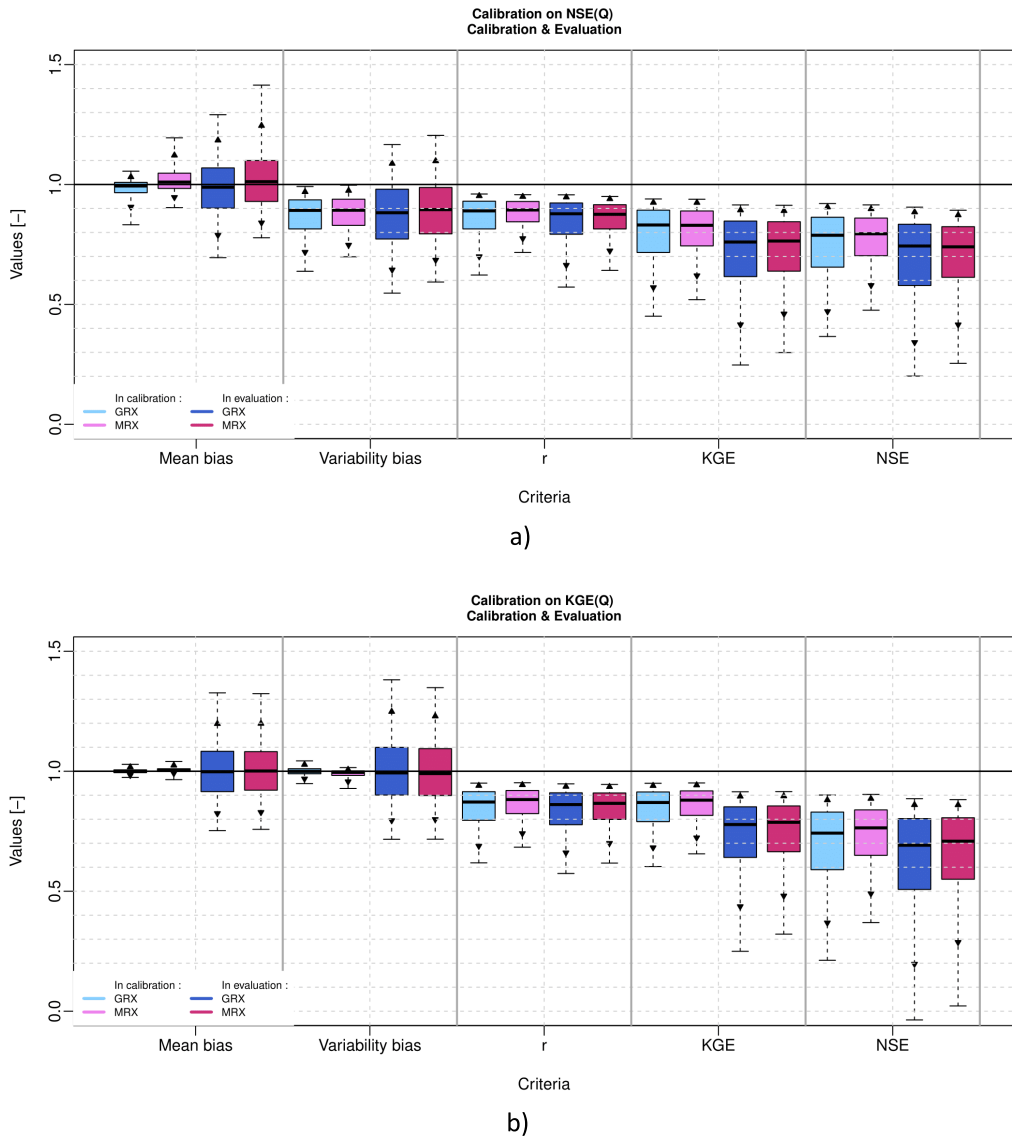


Figure 4. Comparison of GRX and MRX multiobjective performance (mean bias, variability bias, correlation, KGE and NSE) in calibration and evaluation using (a) NSE(Q) or (b) KGE(Q) as objective function to optimize model parameters. Boxplots represent the 5, 10, 25, 50, 75, 90 and 95 quantiles.

In the evaluation period (right-hand-side diagram of Figure 5a), the underestimation of flow variance obviously persists since colored points are still centered around the red semi-circle, though with much more scatter, and bias substantially increases. Two-dimensional contour plots show that 90% of the population lies between $R \in [0.55, 0.97]$ and $\alpha \in [0.4, 1.2]$.

Figure 5b shows the results of GRX model cal-

ibrated with KGE(Q) as objective function. In the calibration period (left-hand-side diagram of Figure 5b), GRX manages to get a small mean bias (red arrows are barely distinguished in the left-hand side diagram of Figure 5b, since they are very short), apart for some particular watersheds (again very arid watersheds). While calibrated with KGE(Q), the centered pattern clearly aligns with the unbiased

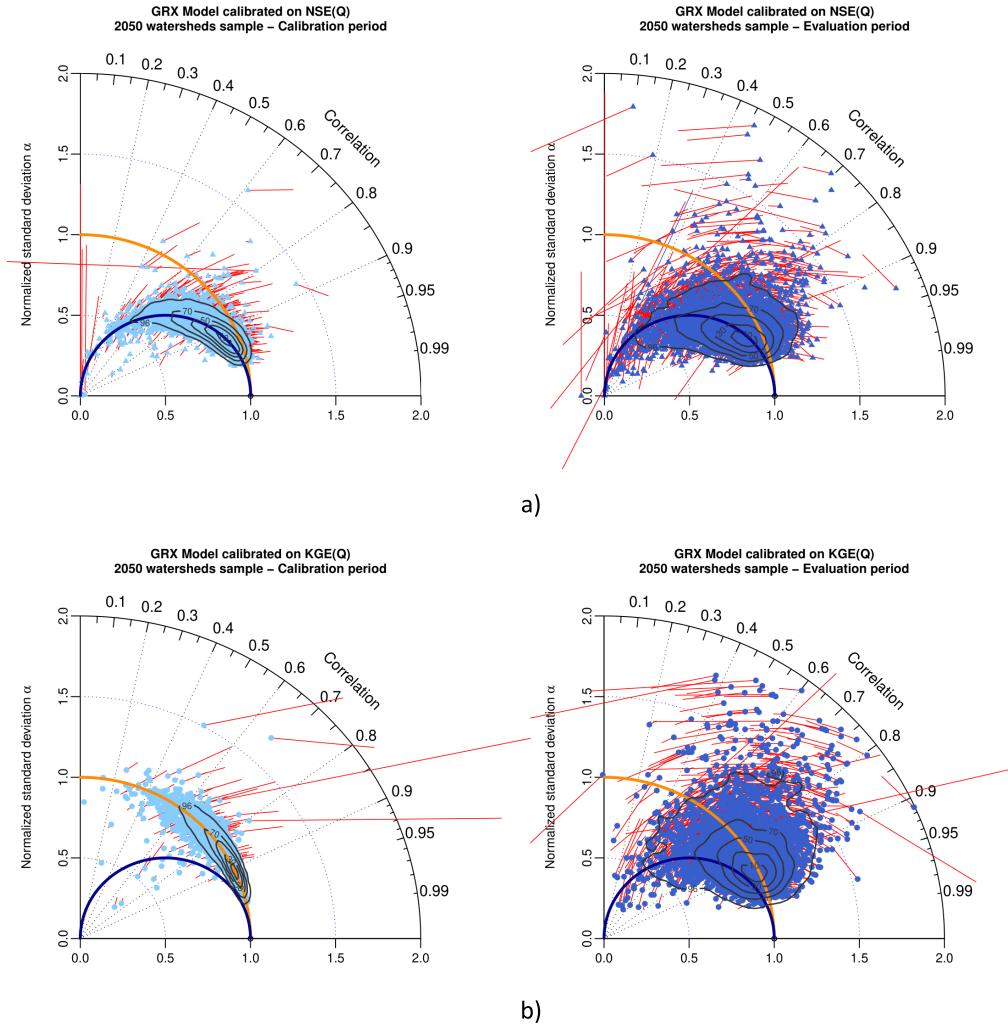


Figure 5. Taylor diagram representing variability bias and correlation (points), and mean bias (arrows in red) for (a) GRX model in calibration (left) and evaluation (right) while calibrated with NSE(Q) as objective function, and (b) GRX model in calibration (left) and evaluation (right), when calibrated with KGE(Q) as objective function. Contour plot illustrate the two-dimensional density of points (from 10% to 90% of the sample).

normalized standard deviation semi-circle (in red) with a very limited 2D scatter (90% of the population lies between $R \in [0.6, 0.98]$ and $\alpha \in [0.95, 1.05]$). In the evaluation period (right-hand-side diagram of Figure 5b), GRX has a limited normalized standard deviation bias since colored points are still centered around the red semi-circle in the (R, α) space, though with much more scatter and bias substantially increases. Two-dimensional contour plots show that 90% of the population lies between

$R \in [0.6, 0.98]$ and $\alpha \in [0.5, 1.5]$.

Figures 6 and 7 present results for NSE(Q) and KGE(Q) as objective functions, for the GRX model and three climate clusters as defined in Mathevet *et al.* [2020]: (a) arid with desert and steppe (A), (b) temperate with warm summer (T+WS), and (c) temperate without dry season and warm summer (T-DS+WS). These figures show that the conclusions obtained with the full 2050 watershed sample are still valid with limited climate clusters (from

100 to 800 watersheds) and patterns of results in the modified Taylor diagram are mostly the same. The large variability of model performance of arid watersheds is illustrated in Figures 6a and 7a, while the homogeneity of model performance for temperate without dry season watersheds is illustrated on Figures 6c and 7c.

As previously shown in Figures 3 and 4, while calibrated with $NSE(Q)$ or $KGE(Q)$, both models have a very similar behavior and level of performances in calibration and evaluation. This is shown by the similar pattern of the 2D density contour plot on Figure 5 (resp. Appendix A, Figure A1), independently from climate clusters as shown on Figures 6 and 7 (resp. Appendix A, Figures A2, A3). The comparison of model behavior clearly shows the significant impact of the choice of the objective function ($NSE(Q)$ or $KGE(Q)$), whatever the hydrological model (GRX or MRX, with very different level of complexity) and whatever watershed properties (large sample of 2050 watersheds worldwide). As stated previously [Gupta et al., 2009, Mathevet et al., 2020, among others], $KGE(Q)$ leads to much more reliable performance than $NSE(Q)$.

Furthermore, the Taylor diagram represents a complementary tool to distributions (Figure 3) or boxplots (Figure 4), allowing a multi-objective representation of model performance behavior on a large sample of watersheds (which is always difficult to summarize) or climate clusters. Taylor diagram (Figures 5–7) allow to display dependency structure between correlation and variability bias while calibrated with $NSE(Q)$.

A complementary use of Taylor diagram is to explore the sub-period variability of performances of a model on a given case study, in comparison to performances estimated over the whole period. As previously explored by Mathevet et al. [2020], sub-period variability of performances could be high, with unbiased simulation in mean and variability at the full period scale, but with a totally different behavior at a sub-period scale. Figure 8 show the full period and sub-period (annual basis) performances for GRX model calibrated with $KGE(Q)$ as objective function for Hérault (Y2102010), Glueyre (V4145210) and Blavet (J5202110) watersheds, during calibration and evaluation. These three watersheds come from the French sample (Banque Hydro stations) and were selected because they represent different types

of climate (Hérault: mediterranean climate with famous “Cévenols” events, Glueyre: mountainous climate, Blavet: oceanic climate) and geological context (Hérault: limestones, Glueyre: granites, metamorphic, volcanic rocks and Blavet: sandstones, metamorphic rocks). Hence, these three watersheds exhibit two different behavior, with a significant sub-period scatter of mean and variability bias for Hérault and Glueyre, while Blavet keep a rather limited and homogeneous mean and variability bias all along time. From calibration to evaluation, sub-period performance patterns exhibited on Taylor diagrams remain mostly the same, with a slight increase of the spread. Taylor diagrams clearly illustrate that even if the overall bias in the calibration or evaluation periods can be quite small, the bias on sub-period intervals can be significant (up to divided/multiplied by 2, on Hérault and Glueyre). These results shows that the use of full-period aggregate performance metrics may not provide sufficient discrimination to properly assess model behavior on sub-periods [Mathevet et al., 2020]. Similar results for MRX are shown in Appendix A, Figure A4.

4.3. *Impact of square root transformation on multi-objective assessment of model performances*

We now present a numerical experiment performed on a limited sample of 635 watersheds (randomly selected). GRX and MRX models were calibrated using a classical mathematical transformation, i.e. square root (RQ) applied to streamflow, using $NSE(Q \& RQ)$ and $KGE(Q \& RQ)$ as objective functions. This transformation is classically used to better represent a larger range of streamflows (i.e. low-flows) and reduce the weight of high-flows during calibration [Pushpalatha et al., 2012]. Another transformation has been tested (log transformation), but results are not shown due to documented numerical issues of this transformation [Santos et al., 2018].

Figure 9 presents Taylor diagrams with GRX model performance in calibration and evaluation for $NSE(Q)$ (a) and $NSE(RQ)$ (b). Figure 10 presents Taylor diagrams with GRX model performance in calibration and evaluation for $KGE(Q)$ (a) and $KGE(RQ)$ (b). Similar results for MRX are shown in Appendix A, Figures A5 and A6.

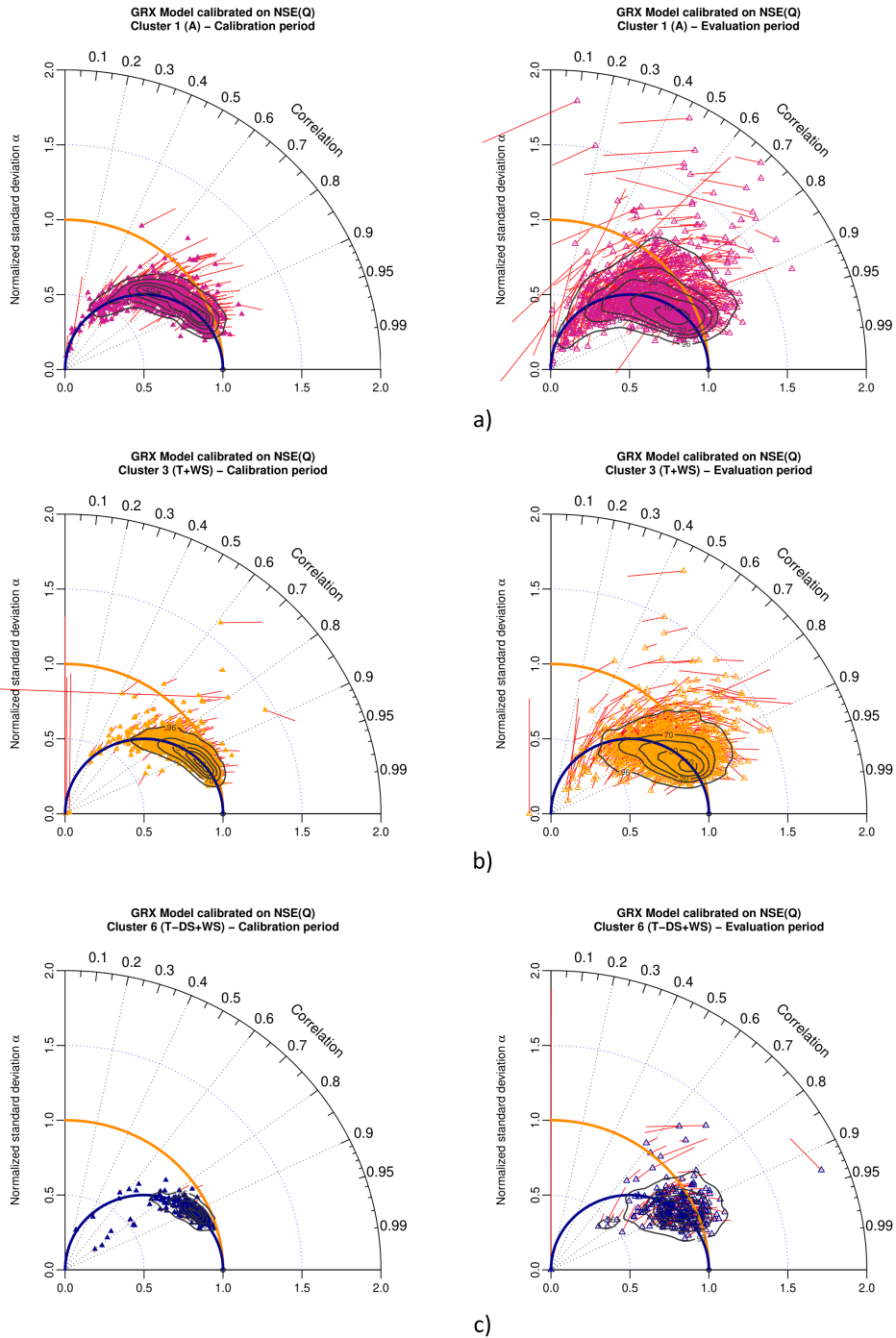


Figure 6. Taylor diagram representing variability bias and correlation (points) and mean bias (red arrows) for GRX model in calibration (left) and evaluation (right) for (a) arid with desert and steppe cluster (586 watersheds), (b) temperate with warm summer cluster (785 watersheds), and (c) temperate without dry season and warm summer (125 watersheds), when calibrated with NSE(Q) as objective function. Contour plots illustrate the two-dimensional density of points (from 10% to 90% of the sample).

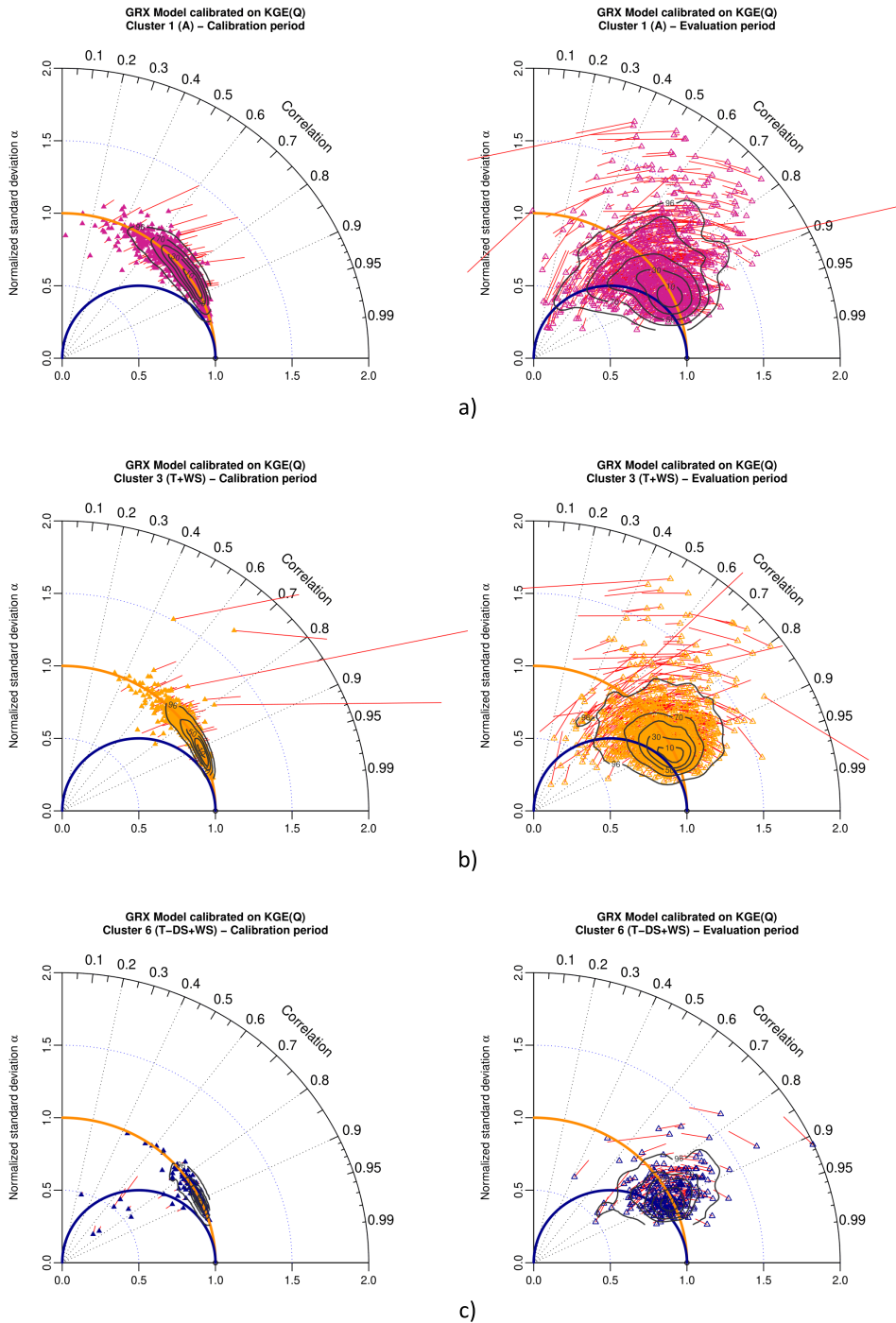


Figure 7. Taylor diagram representing variability bias and correlation (points) and mean bias (red arrows) for GRX model in calibration (left) and evaluation (right) for (a) arid with desert and steppe cluster (586 watersheds), (b) temperate with warm summer cluster (785 watersheds) and (c) temperate without dry season and warm summer (125 watersheds), when calibrated with KGE(Q) as objective function. Contour plots illustrate the two-dimensional density of points (from 10% to 90% of the sample).

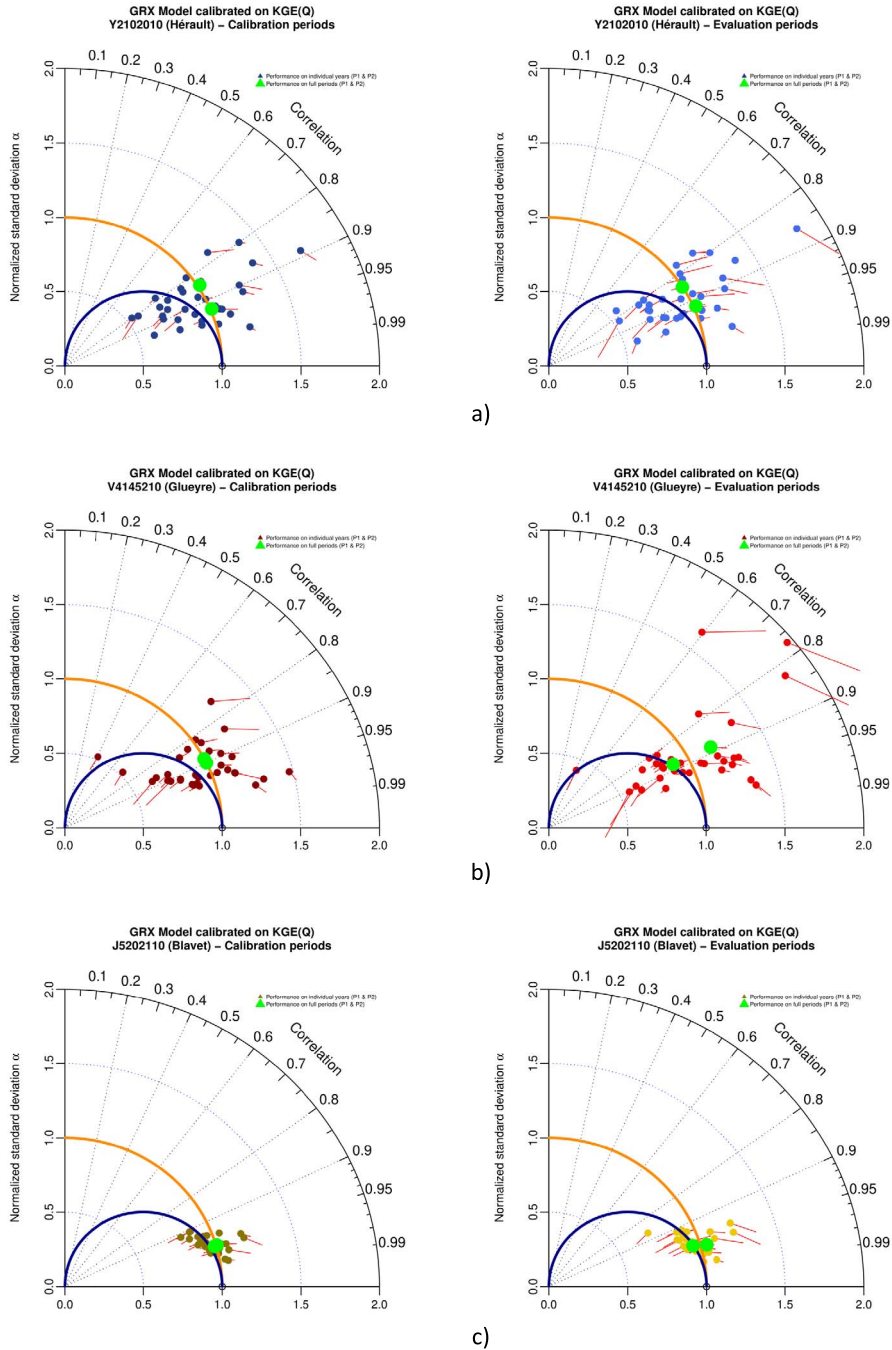


Figure 8. Taylor diagram representing variability bias and correlation (points) and mean bias (red arrows) for GRX model in calibration (left) and evaluation (right) for (a) Hérault watershed, (b) Glueyre watershed and (c) Blavet watershed, when calibrated with KGE(Q) as objective function. Points either represent performances on individual years (color) or on the full periods (green color). These three watersheds had been selected because generations of Ghislain de Marsily and Pierre Hubert students (DEA National d’Hydrologie) swan, practiced kayak or celebrate New socio-hydrological years (NASH) in their beautiful waters.

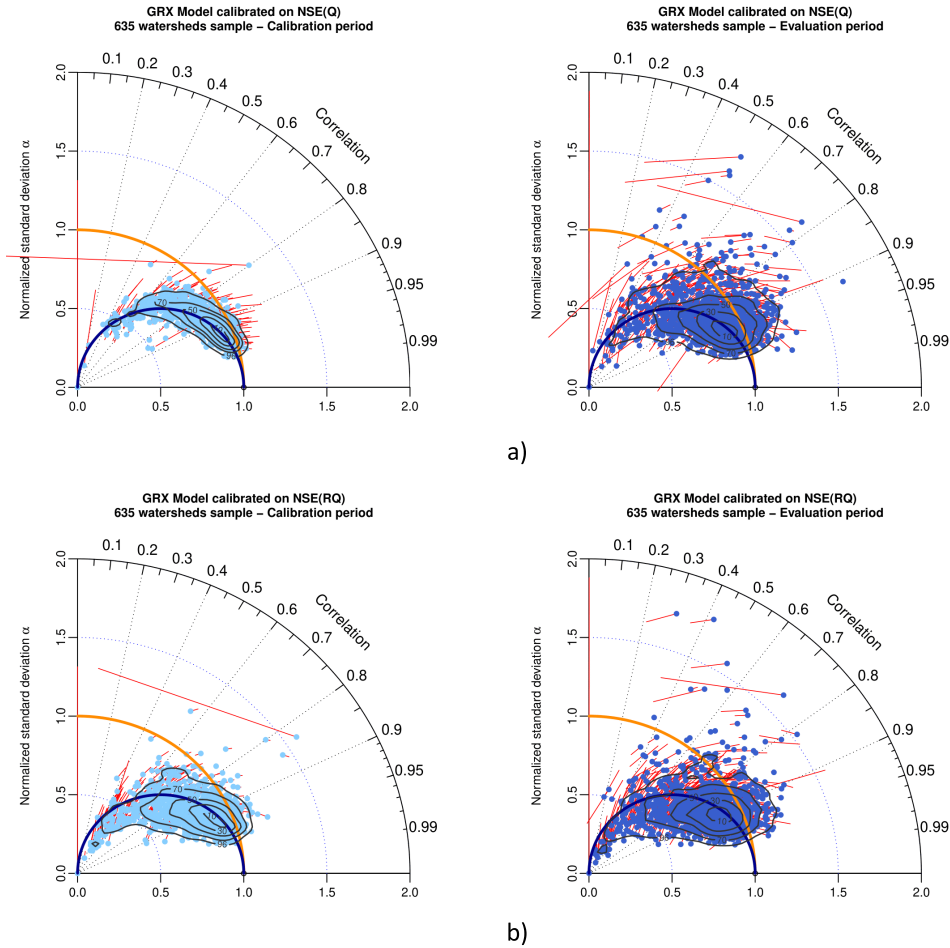


Figure 9. Taylor diagram representing variability bias and correlation (points) and mean bias (red arrows) for GRX model in calibration (left) and evaluation (right), when calibrated with (a) NSE(Q) and (b) NSE(RQ) as objective function. The contour plot illustrates the two-dimensional density of points (from 10% to 90% of the sample).

When using the NSE metric as objective function for parameter optimization, in calibration, Figure 9b left (square root transformation) compared to Figure 9a left (natural streamflow) shows that this classical numerical transformation of streamflow increases the normalized standard deviation bias, with a majority of points located slightly to significantly under the blue semi-circle line with an increasing spread, for square root transformation of streamflow. Two-dimension contour plots surface of 90% of the population increase from NSE(Q) to NSE(RQ). In evaluation, Figure 9b right (square root transformation), compared to Figure 9a right (natural streamflow) shows that the pattern found in calibration re-

main the same concerning the normalized standard deviation bias, with an increase of the spread of the results (as shown by the two-dimensional contour plots surface of 90% of the population).

When using the KGE metric as objective function for parameter optimization, in calibration, Figure 10b left (square root transformation) compared to Figure 10a left (natural streamflow) shows that this classical numerical transformation of streamflow increases the normalized standard deviation bias, with a majority of points located between the red semi-circle line and the blue semi-circle line for square root transformation. The spread of the results increases slightly for square root transformation. Two-

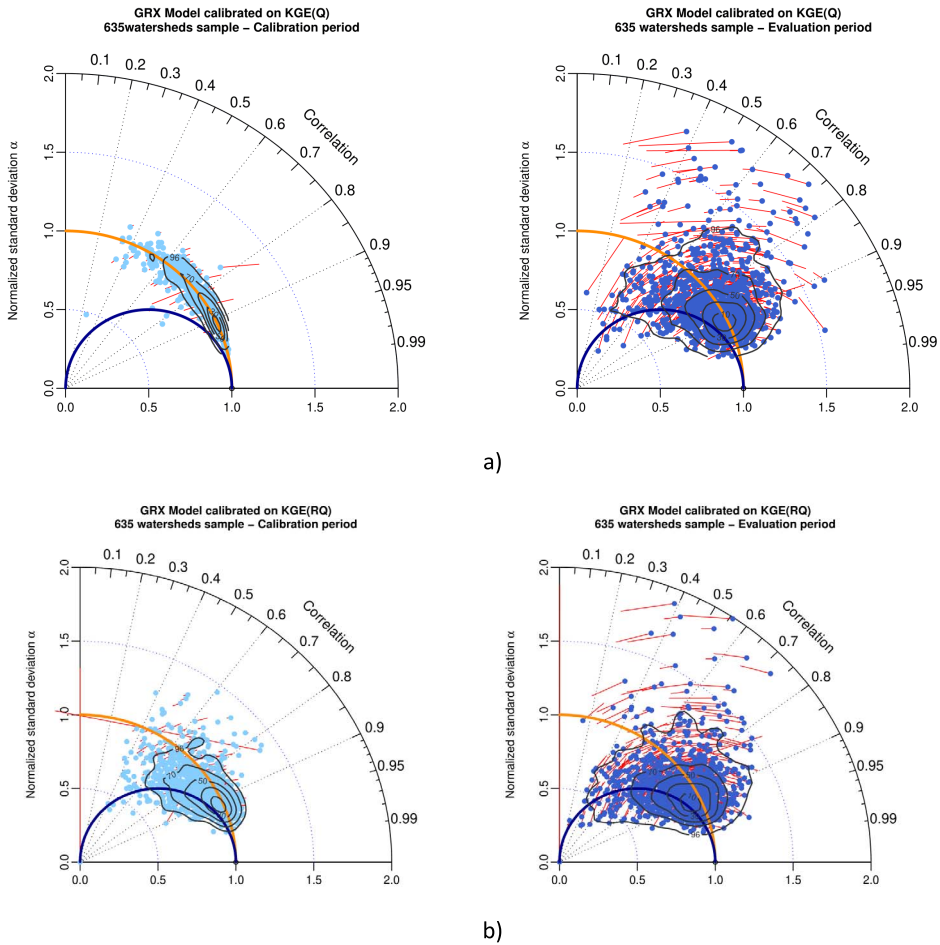


Figure 10. Taylor diagram representing variability bias and correlation (points) and mean bias (red arrows) for GRX model in calibration (left) and evaluation (right), while calibrated with (a) KGE(Q) and (b) KGE(RQ) as objective function. The contour plot illustrates the two-dimensional density of points (from 10% to 90% of the sample).

dimension contour plots surface of 90% of the population increases from KGE(Q) to KGE(RQ). In evaluation, Figure 10b right (square root transformation) compared to Figure 10a right (natural streamflow) shows that the pattern found in calibration remain the same concerning the normalized standard deviation bias, with an increase of the spread of the results (as shown by the two-dimensional contour plots surface of 90% of the population).

Comparison of Figure 9a (calibration with NSE(Q)), Figure 10a (calibration on KGE(Q)) and Figure 10b (calibration on KGE(RQ)) allows to compare patterns of results (in calibration and evalu-

ation) for different objective functions. Concerning the variability bias, this comparison shows that pattern of calibration with KGE(RQ) lies in-between patterns of KGE(Q) (no bias) and NSE(Q) ($\alpha = R$).

5. Discussion

Based on a worldwide sample of 2050 watersheds, two conceptual rainfall-runoff models (GRX and MRX), two metrics classically used in hydrology

(Nash–Sutcliffe efficiency and Kling–Gupta efficiency) and a split sample test, this paper investigated the usefulness of a modified Taylor diagram to analyze the results of large sample experiments.

We first proposed a modified Taylor diagram to make clear the theoretical reasons why OLS schemes tend to bias model simulations towards an underestimated standard deviation of streamflows. Empirical evidence of this behavior was provided in an intensive numerical experiment over a large watershed sample. NSE(Q) is still largely used by hydrological modelers and we encourage the use of KGE(Q) instead of NSE(Q). The clear advantage of KGE(Q) instead of NSE(Q) is that it deals with the optimization process involving several objective functions (correlation, ratio of means, and ratio of standard deviations) independently while NSE(Q) implicitly involved a prescribed trade-off between correlation and ratio of standard deviation. As a consequence, we showed that calibrating hydrological models with NSE(Q) led to significant variability biases on watersheds where models have difficulties representing the temporal behavior of the watershed. KGE(Q) tended to reduce long-term mean and variability bias, independently from the models' level of correlation. These problems related to NSE (and more generally to OLS schemes) were already reported in previous studies [see e.g. Gupta et al., 2009] but the illustration provided by the modified Taylor diagram is a valuable add-on to these studies. Besides these numerical problems, NSE does put more weight on high flows, in the sense that high flow days have a major contribution to the total squared error. As with all least-squares-based schemes, using NSE implicitly considers uncorrelated error time series and homoscedastic errors [see e.g. Kavetski et al., 2003] and thus does not use the whole information concerning the temporal structure of the observed discharge time series. KGE allows to partially cope with this problem by including more explicitly the errors in variance. Other smarter error models (e.g. weighted least square accounting for heteroscedasticity or correlation in the residuals) may be considered and visualizing their optimization results under the proposed Taylor diagram may help to understand how the trade-off between correlation, the ratio of means, and the ratio of standard deviation are modified compared to NSE(Q) or KGE(Q).

Interestingly, we showed that the biased optimization of OLS schemes towards reduced streamflow variability was independent on the model used and the environmental settings of the watersheds. When modeling a single watershed, modified Taylor diagrams can be represented for all hydrological years individually since the use of full-period aggregate performance metrics may not provide sufficient discrimination to properly assess model behavior on sub-periods. Figure 8 showed that the optimization process may be different according to the studied watershed in the way it deals with annual biases and compensation along the calibration period. Thus, we believe that the modified Taylor diagram can be an interesting tool to investigate the ability of the model to reproduce individual years, in complement to other existing graphical tools [see e.g. Coron et al., 2015]. This diagnosis allows the modelers to figure out the ability of the model for extrapolation.

Last, we showed that calibrating hydrological models with NSE metric applied to square root of streamflows increases the initial pitfalls of using the NSE metric on natural streamflow. This transformation increases the normalized standard deviation bias of simulations while increasing the spread of the results in the (R, α) space. It is also shown that calibrating hydrological models with KGE metric applied to the square root of streamflow reduces the benefits of using the KGE metric on streamflow. Again, this transformation increases the normalized standard deviation bias of simulations, while increasing the spread of the results in the (R, α) space. As stated before [Santos et al., 2018], we consider that using KGE metric on square root has significant drawbacks and should be avoided since the main drawbacks of the NSE metric are introduced again.

6. Conclusion

We proposed in this paper a novel diagnostic tool for hydrological model simulations. The proposed graphical tool is based on the Taylor diagram and we adapted this diagram to visualize commonly used assessment criteria in hydrological modeling.

The adapted Taylor diagram illustrates some well-known drawbacks of OLS schemes widely used in the scientific community and particularly the fact that the standard deviation of the simulated streamflow

is systematically underestimated. While the use of alternative objective functions such as the KGE(Q) overcomes these problems, future works may investigate the outputs of hydrological models optimized with other objective functions that consider heteroscedasticity and/or based on flow signatures. Representing the outputs of these more complex objective functions into the modified Taylor diagram may help to understand how the calibration process deals with the trade-off between correlation, the ratio of standard deviation, and the ratio of means.

Conflicts of interest

Authors have no conflict of interest to declare.

Acknowledgements

Authors would like to thank Charles Perrin for his valuable support and constructive comments on the manuscript. Authors would like to warmly acknowledge Editors for their invitation to contribute to this special issue and the three anonymous reviewers for their very constructive remarks.

Authors acknowledge: Météo France, SCHAPI-Banque Hydro, EDF, Laurent Coron, Nicolas Le Moine and Audrey Valery for the French data sets, Jai Vaze and Francis Chiew for the Australian data sets (CSIRO), John Schaake and Qingyun Duan for the American (MOPEX) data set, Audrey Valery for the Swiss (Météo Suisse and OFEV) and Swedish (SMHI) data sets, Berit Arheimer for the Swedish (SMHI) data sets, and Barry Croke and Ian Littlewood for the English data sets (TDMWG).

Codes used to produce Taylor diagrams of this paper will be made available in the airGR package [Coron *et al.*, 2017, 2022].

Appendix A.

Appendix A shows the results for MRX model of numerical experiments:

- Figure A1 (corresponding to Figure 11 for GRX): Taylor diagram for calibration with NSE(Q) and MSE(Q);

- Figure A2 (corresponding to Figure 12 for GRX): Taylor diagram for calibration with NSE(Q) for 3 different climate clusters;
- Figure A3 (corresponding to Figure 13 for GRX): Taylor diagram for calibration with KGE(Q) for 3 different climate clusters;
- Figure A4 (corresponding to Figure 14 for GRX): Taylor diagram for calibration with KGE(Q) for 3 different watersheds in France (Hérault, Glueyre and Blavet);
- Figure A5 (corresponding to Figure 15 for GRX): Taylor diagram for calibration with NSE(Q) and NSE(RQ);
- Figure A6 (corresponding to Figure 16 for GRX): Taylor diagram for calibration with KGE(Q) and KGE(RQ).

These figures show that numerical experiments with MRX model lead to similar results and conclusions to those obtained with GRX model (patterns on Taylor diagrams are very similar). These analyses with GRX and MRX models confirm the generality of our results, independent from the rainfall-runoff model structure.

References

- Addor, N., Do, H. X., Alvarez-Garreton, C., Coxon, G., Fowler, K., and Mendoza, P. A. (2020). Large-sample hydrology: recent progress, guidelines for new datasets and grand challenges. *Hydrol. Sci. J.*, 65(5), 712–725.
- Andréassian, V. (2023). On the (im)possible validation of hydrogeological models. *C. R. Géosci.*, 355(S1). Online first.
- Coron, L., Andréassian, V., Perrin, C., and Le Moine, N. (2015). Graphical tools based on Turc–Budyko plots to detect changes in catchment behaviour. *Hydrol. Sci. J.*, 60, 1394–1407.
- Coron, L., Delaigue, O., Thirel, G., Dorchies, D., Perrin, C., and Michel, C. (2022). airGR: suite of GR hydrological models for precipitation-runoff modelling. <https://CRAN.R-project.org/package=airGR>. R package version 1.7.0.
- Coron, L., Thirel, G., Delaigue, O., Perrin, C., and Andréassian, V. (2017). The suite of lumped GR hydrological models in an R package. *Environ. Modell. Softw.*, 94, 166–171.

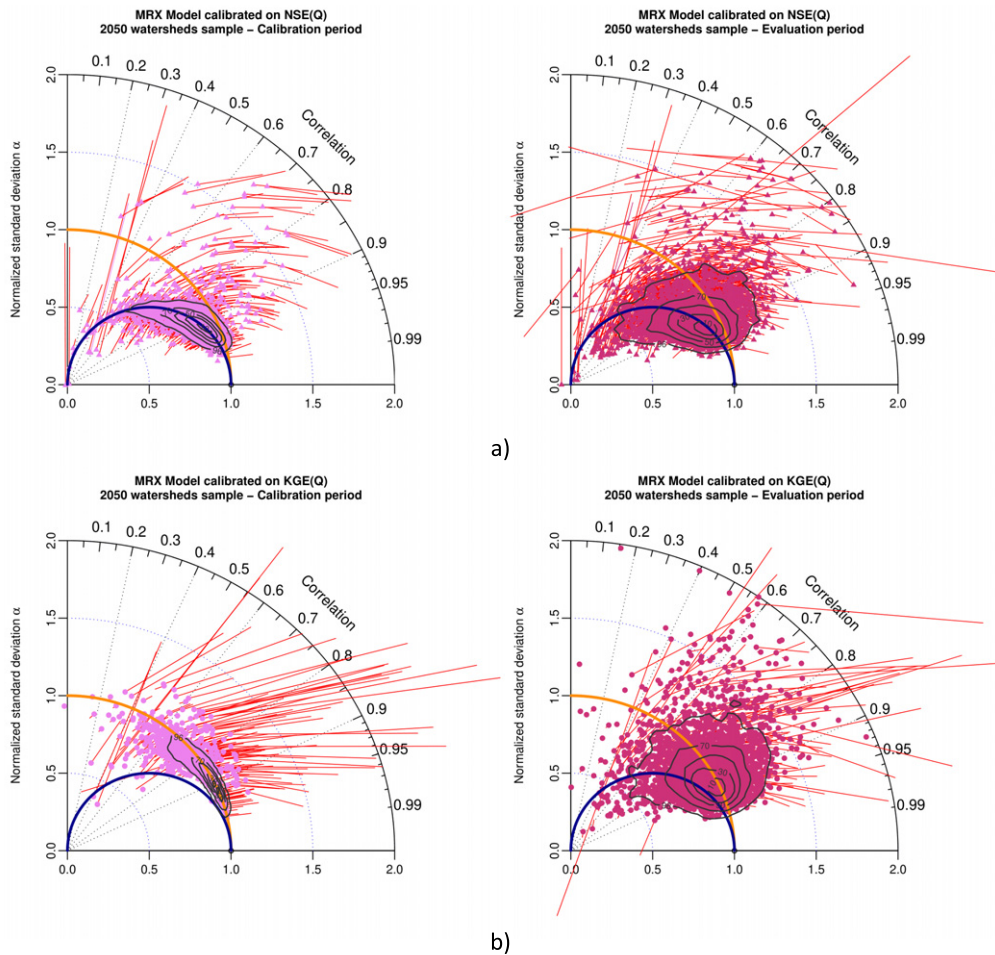


Figure A1. Taylor diagram representing variability bias and correlation (points) and mean bias (arrows in red) for (a) MRX model in calibration (left) and evaluation (right) while calibrated with NSE(Q) as objective function, and (b) MRX model in calibration (left) and evaluation (right), when calibrated with KGE(Q) as objective function. Contour plots illustrate the two-dimensional density of points (from 10% to 90% of the sample).

de Marsily, G. (1994). Quelques réflexions sur l'utilisation des modèles en hydrologie. [Tribune libre]. *Revue des sciences de l'eau / J. Water Sci.*, 7(3), 219–234.

Garavaglia, F., Le Lay, M., Gottardi, F., Garçon, R., Gailhard, J., Paquet, E., and Mathevet, T. (2017). Impact of model structure on flow simulation and hydrological realism: from a lumped to a semi-distributed approach. *Hydrol. Earth Syst. Sci.*, 21, 3937–3952.

Garçon, R. (1996). Prévision opérationnelle des ap-

ports de la Durance à Serre-Ponçon à l'aide du modèle MORDOR. Bilan de l'année 1994–1995. *Houille Blanche*, 5, 71–76.

Gupta, H. V., Kling, H., Yilmaz, K. K., and Martinez-Baquero, G. F. (2009). Decomposition of the mean squared error & NSE performance criteria: implications for improving hydrological modelling. *J. Hydrol.*, 377, 80–91.

Gupta, H. V., Perrin, C., Blöschl, G., Montanari, A., Kumar, R., Clark, M., and Andréassian, V. (2014). Large-sample hydrology: a need to balance depth

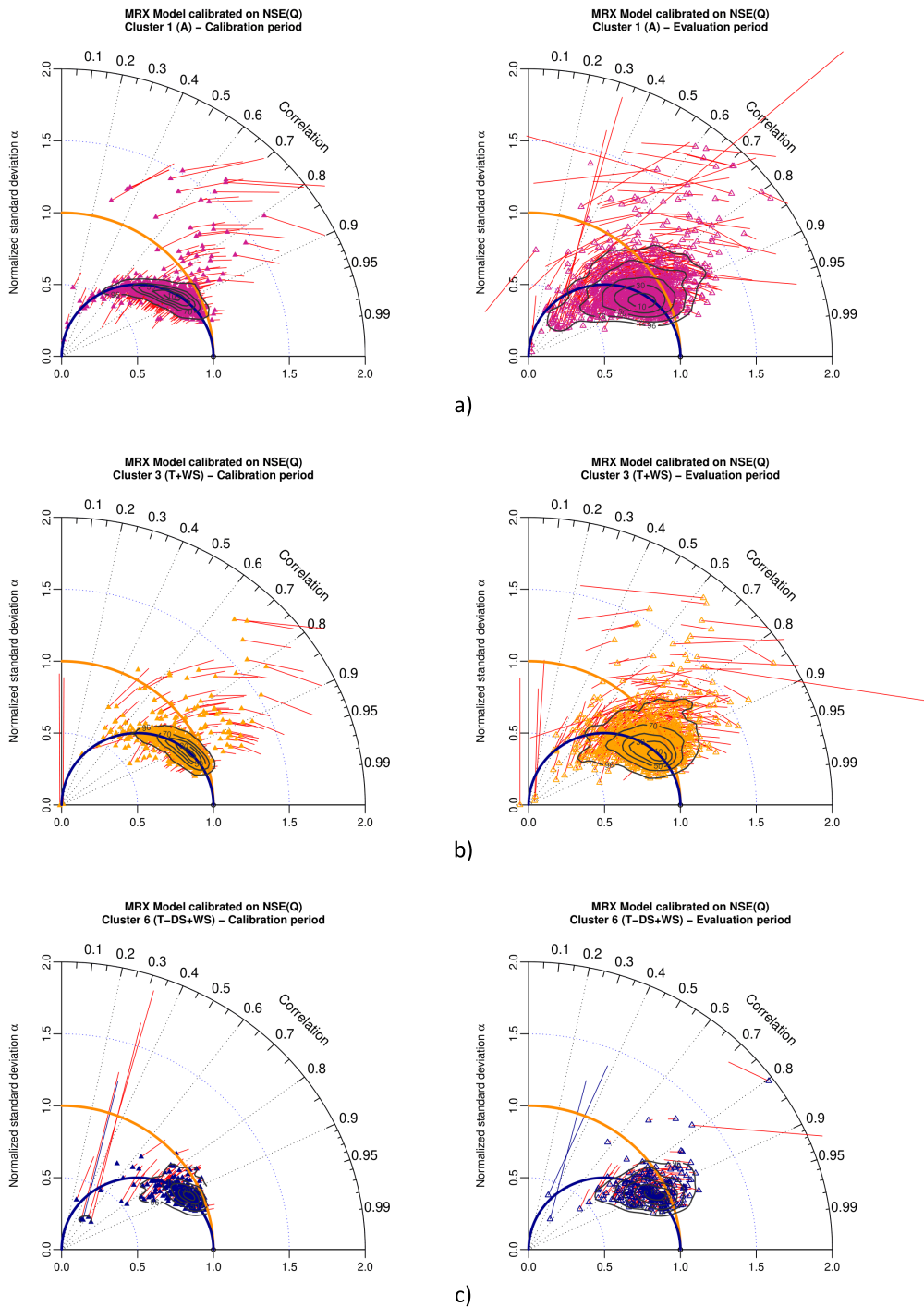


Figure A2. Taylor diagram representing variability bias and correlation (points) and mean bias (red arrows) for MRX model in calibration (left) and evaluation (right) for (a) arid with desert and steppe cluster (586 watersheds), (b) temperate with warm summer cluster (785 watersheds) and (c) temperate without dry season and warm summer (125 watersheds), when calibrated with NSE(Q) as objective function. Contour plots illustrate the two-dimensional density of points (from 10% to 90% of the sample).

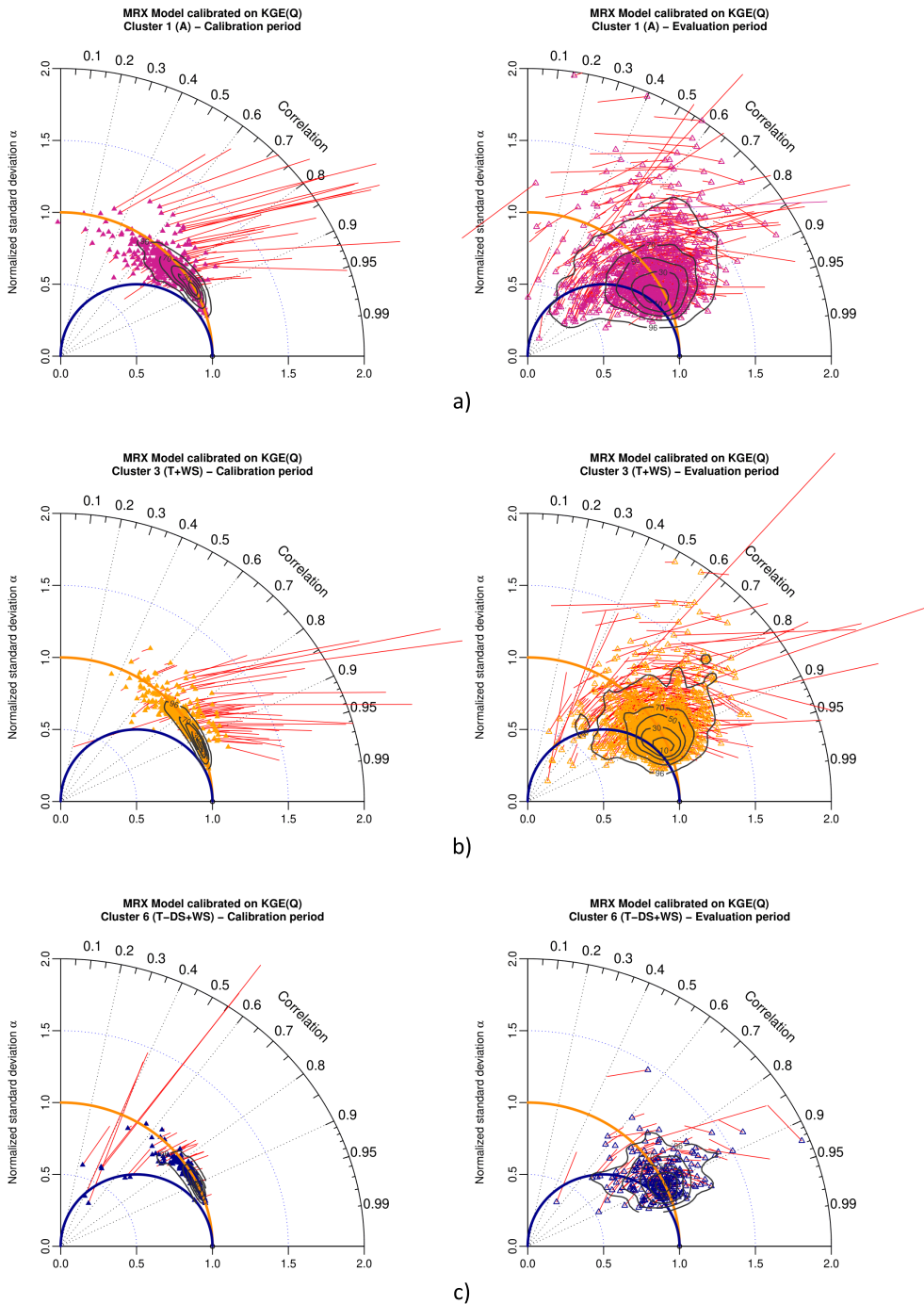


Figure A3. Taylor diagram representing variability bias and correlation (points) and mean bias (red arrows) for MRX model in calibration (left) and evaluation (right) for (a) arid with desert and steppe cluster (586 watersheds), (b) temperate with warm summer cluster (785 watersheds) and (c) temperate without dry season and warm summer (125 watersheds), when calibrated with KGE(Q) as objective function. Contour plots illustrate the two-dimensional density of points (from 10% to 90% of the sample).

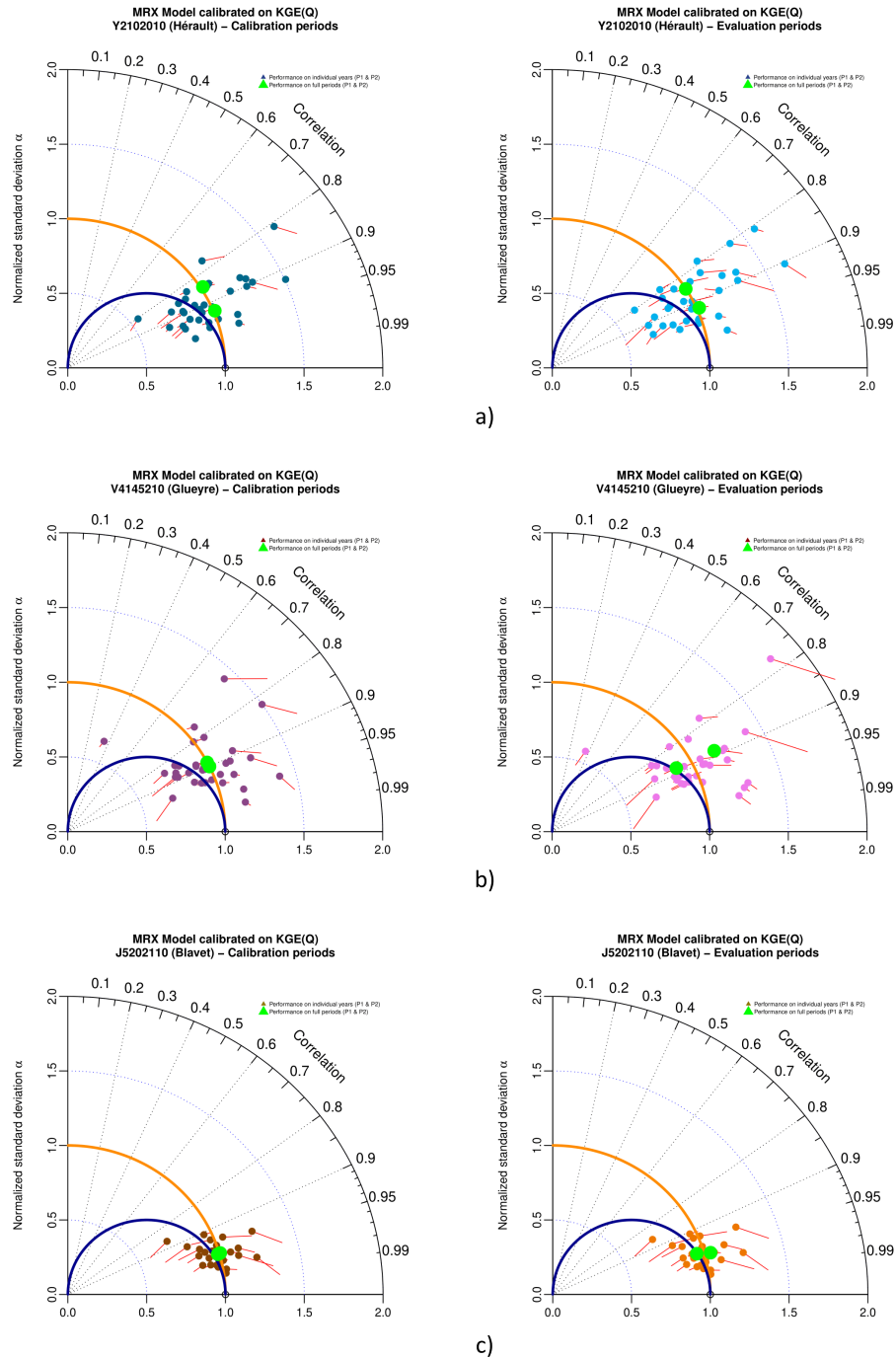


Figure A4. Taylor diagram representing KGE mean bias, variability bias and correlation for MRX model in calibration (left) and evaluation (right) for (a) Hérault watershed, (b) Glueyre watershed and (c) Blavet watershed, while calibrated with KGE(Q) as objective function. Points either represent performances on individual years (color) or on the full periods (green color). These three watersheds had been selected because generations of Ghislain de Marsily and Pierre Hubert students (DEA National d'Hydrologie) swan, practiced kayak or celebrate New socio-hydrological years (NASH) in their beautiful waters.

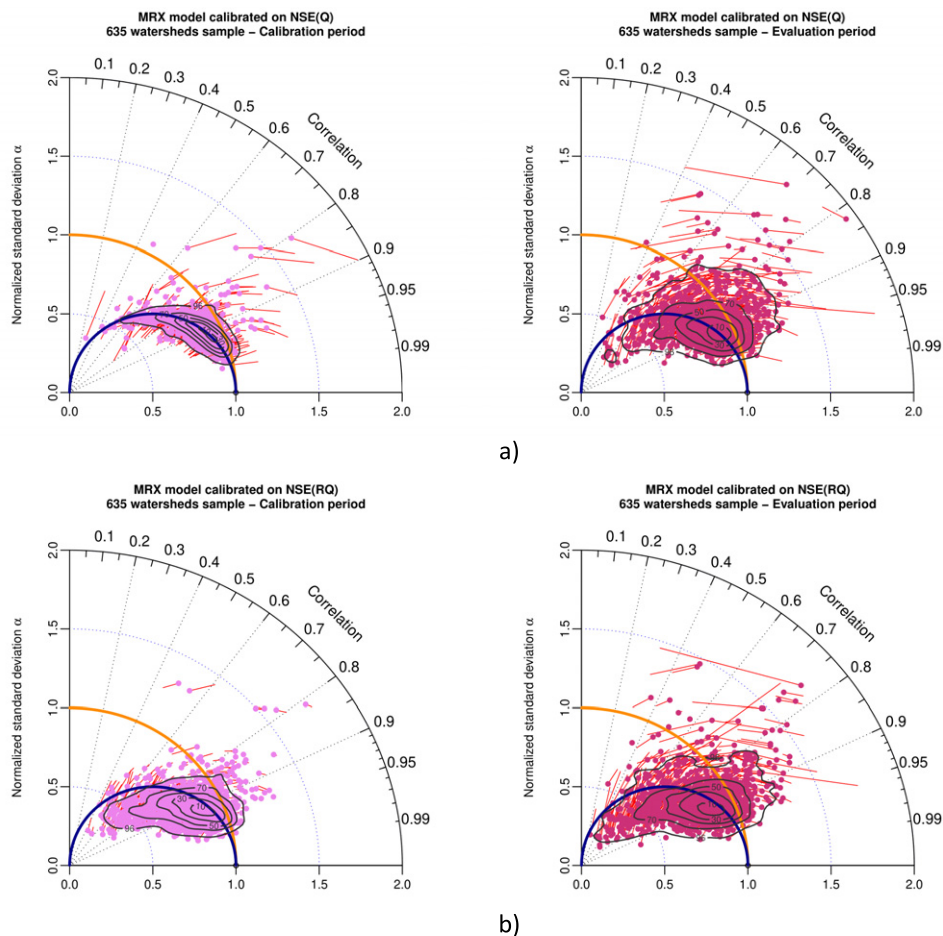


Figure A5. Taylor diagram representing variability bias and correlation (points) and mean bias (red arrows) for MRX model in calibration (left) and evaluation (right), when calibrated with (a) NSE(Q) and (b) NSE(RQ) as objective function. The contour plot illustrates the two-dimensional density of points (from 10% to 90% of the sample).

with breadth. *Hydrol. Earth Syst. Sci.*, 18, 463–477.

Kavetski, D., Franks, S. W., and Kuczera, G. (2003). Confronting input uncertainty in environmental modelling. In Duan, Q., Gupta, V. H., Sorooshian, S., Rousseau, N. A., and Turcotte, R., editors, *Calibration of Watershed Models*. American Geophysical Union, Washington, DC.

Klemeš, V. (1986). Operational testing of hydrological simulation models. *Hydrol. Sci. J.*, 31(1), 13–24.

Konikow, L. F. and Bredehoeft, J. D. (1992). Groundwater models cannot be validated. *Adv. Water Resour.*, 15, 75–83.

Lane, R. A., Coxon, G., Freer, J. E., Wagener, T., Johnes,

P. J., Bloomfield, J. P., Greene, S., Macleod, C. J. A., and Reaney, S. M. (2019). Benchmarking the predictive capability of hydrological models for river flow and flood peak predictions across over 1000 catchments in Great Britain. *Hydrol. Earth Syst. Sci.*, 23, 4011–4032.

Le Moine, N. (2008). *Le bassin versant de surface vu par le souterrain : une voie d'amélioration des performances et du réalisme des modèles pluie-débit ?* Thèse de doctorat, Université Pierre et Marie Curie (Paris), Cemagref (Antony). 324 pages.

Maroufpoor, S., Bozorg-haddad, O., and Maroufpoor, E. (2020). Reference evapotranspiration estimating

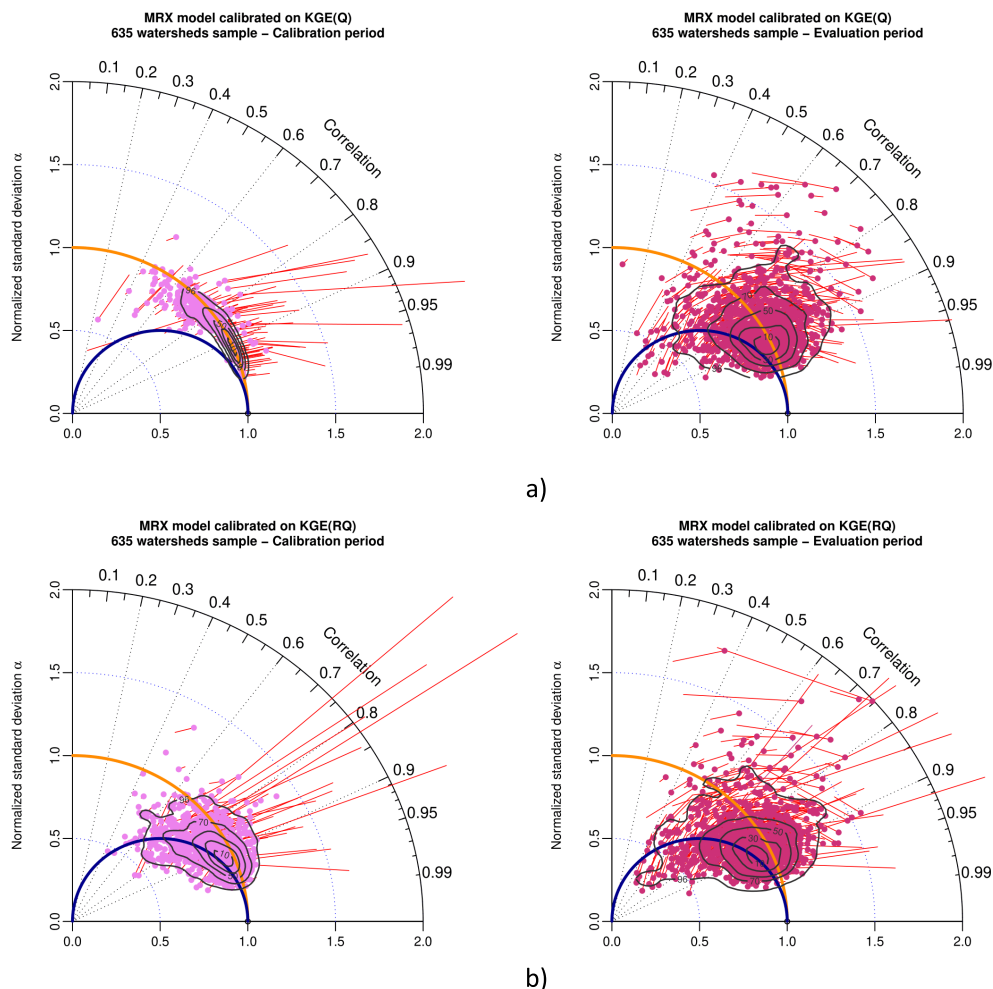


Figure A6. Taylor diagram representing variability bias and correlation (points) and mean bias (red arrows) for MRX model in calibration (left) and evaluation (right), when calibrated with (a) KGE(Q) and (b) KGE(RQ) as objective function. The contour plot illustrates the two-dimensional density of points (from 10% to 90% of the sample).

based on optimal input combination and hybrid artificial intelligent model: hybridization of artificial neural network with grey wolf optimizer algorithm. *J. Hydrol.*, 588, article no. 125060.

Mathevet, T. (2005). *Quels modèles pluie-débit globaux pour le pas de temps horaire ? Développement empirique et comparaison de modèles sur un large échantillon de bassins versants*. Thèse de doctorat, ENGREF (Paris), Cemagref (Antony), France. 463 pages.

Mathevet, T., Gupta, H., Perrin, C., Andréassian, V., and Le Moine, N. (2020). Assessing the perfor-

mance and robustness of two conceptual rainfall-runoff models on a worldwide sample of watersheds. *J. Hydrol.*, 585, article no. 124698.

Mathevet, T., Michel, C., Andréassian, V., and Perrin, C. (2006). *A Bounded Version of the Nash-Sutcliffe Criterion for Better Model Assessment on Large Sets of Basins*. IAHS Red Books Series No 307. IAHS, Wallingford, Oxfordshire, UK.

McMillan, H. K., Booker, D. J., and Cattoën, C. (2016). Validation of a national hydrological model. *J. Hydrol.*, 541, 800–815.

Nash, J. and Sutcliffe, J. (1970). River flow forecasting

- through conceptual models part I. A discussion of principles. *J. Hydrol.*, 10, 282–290.
- Newman, A. J., Clark, M. P., Sampson, K., Wood, A., Hay, L. E., Bock, A., Viger, R. J., Blodgett, D., Brekke, L., Arnold, J. R., Hopson, T., and Duan, Q. (2015). Development of a large-sample watershed-scale hydrometeorological data set for the contiguous USA: data set characteristics and assessment of regional variability in hydrologic model performance. *Hydrol. Earth Syst. Sci.*, 19, 209–223.
- Oudin, L., Hervieu, E., Michel, C., Perrin, C., Andréassian, V., Anctil, E., and Loumagne, C. (2005). Which potential evapotranspiration input for a lumped rainfall-runoff model?: Part 2—Towards a simple and efficient potential evapotranspiration model for rainfall-runoff modelling. *J. Hydrol.*, 303, 290–306.
- Pushpalatha, R., Perrin, C., Le Moine, N., and Andréassian, V. (2012). A review of efficiency criteria suitable for evaluating low-flow simulations. *J. Hydrol.*, 420–421, 171–182.
- Pushpalatha, R., Perrin, C., Le Moine, N., Mathevet, T., and Andréassian, V. (2011). A downward structural sensitivity analysis of hydrological models to improve low-flow simulation. *J. Hydrol.*, 411(1–2), 66–76.
- Santos, L., Thirel, G., and Perrin, C. (2018). Technical note: pitfalls in using log-transformed flows within the KGE criterion. *Hydrol. Earth Syst. Sci.*, 22, 4583–4591.
- Schaefli, B. and Gupta, H. V. (2007). Do Nash values have value? *Hydrol. Process.*, 21, 2075–2080.
- Taylor, K. E. (2001). Summarizing multiple aspects of model performance in a single diagram. *J. Geophys. Res.*, 106(D7), 7183–7192.
- Yaseen, Z. M., Awadh, S. M., Sharafati, A., and Shahid, S. (2018). Complementary data-intelligence model for river flow simulation. *J. Hydrol.*, 567, 180–190.